Characterization of platinum nitride from first-principles calculations

J. Phys.: Condens. Matter **21** (2009) 485403 (8pp) doi:10.1088/0953-8984/21/48/485403

Characterization of platinum nitride from first-principles calculations

A Yıldız[1], Ü Akıncı[1], O Gülseren[2] and İ Sökmen[1]

[1] Physics Department, Dokuz Eylül University, İzmir 35160, Turkey
[2] Department of Physics, Bilkent University, Ankara 06800, Turkey

E-mail: gulseren@fen.bilkent.edu.tr

Received 15 July 2009, in final form 2 October 2009
Published 30 October 2009
Online at stacks.iop.org/JPhysCM/21/485403

Abstract

We have performed a systematic study of the ground state properties of the zinc-blende, rock-salt, tetragonal, cuprite, fluorite and pyrite phases of platinum nitride by using the plane wave pseudopotential calculations within the density functional theory. The equilibrium structural parameters and bulk moduli are computed within both the local density approximation (LDA) and generalized gradient approximation (GGA). The comparison of the equation of state (EOS) calculated within the LDA for the pyrite structure with the experimental results demonstrates an excellent agreement, hence the use of the LDA rather than the GGA is essential. Complete sets of elastic moduli are presented for cubic forms. The analysis of the results reveal that the pyrite phase with PtN_2 stoichiometry leads to the formation of a hard material with the shear modulus $G = 206$ GPa. The electronic structure of pyrite PtN_2 is given, which shows a narrow indirect gap. The vibrational properties of platinum nitride are investigated in detail from lattice dynamical calculations. The calculations show that fluorite and pyrite structures are dynamically stable as well. However, the calculated vibrational modes of pyrite PtN_2 do not show complete agreement with experimental Raman frequencies.

1. Introduction

The transition metal nitrides are well known for possessing a number of extreme and useful resilient properties. They have traditionally been used as coatings to protect mechanical tools, such as bits and drills, because of their hardness, brittleness and high melting points. Most of the early transition metal nitrides are also reported as superconductors. The new nitrides have enabled the use of Cooper interconnects in integrated circuits through the creation of improved diffusion barriers, thus paving the way for a new generation of faster computer chips. Therefore the interest in the synthesis of transition metal nitrides has grown considerably during the past decade [1–3].

Recently, Gregoryanz *et al* [1] managed to synthesize platinum nitride, the first noble metal nitride. The new crystalline compound was formed using a laser-heated diamond anvil cell set-up at temperatures above 2000 K and pressures of 50 GPa. The system was quenched to atmospheric pressure and room temperature and then was characterized by Raman spectroscopy and synchrotron x-ray diffraction. The platinum nitride has cubic structure ($a = 4.8041(2)$ Å at 0.1 MPa) where metal atoms form an fcc lattice, while the occupation sites of nitrogen atoms could not be clarified because of the large mass difference between platinum and nitrogen. This binary nitride was determined to have a remarkably high bulk modulus (B) of 372($\pm$5) GPa, which is 100 GPa higher than that of bulk Pt ($\approx$270 GPa). This is comparable with the $B = 382(\pm3)$ GPa of the superhard cubic material BN [4]. The measured Raman spectrum exhibited a strong longitudinal optic (LO) mode and weaker transverse optic (TO) mode. The frequencies of modes are shown to increase almost linearly with pressure [1]. It was also determined that platinum nitride is not superconducting (down to 2 K) and it was suggested the material be either a poor metal or semiconductor with a small bandgap. Later experiments performed by Crowhurst *et al* [2] report similar synthesis conditions to [1]. They measured two intense Raman modes at around 860 and 1020 cm^{-1}, with two weaker modes at 790 and 1050 cm^{-1} in the Raman spectrum after the reaction under the pressure environment.

The desire to understand such properties has stimulated a large number of theoretical investigations of structural properties and electronic structure of platinum nitride [5–23]. According to Rietveld refinement, early predictions were that

the structure of platinum nitride can be of zinc-blende as well as rock-salt type. But the rock-salt structure was ruled out because of the observed first-order Raman spectrum. Many studies [6–11] showed that platinum nitride is unstable with the zinc-blende structure and reported much lower values for bulk modulus than its experimental value. Recently, Yu and Zhang [9, 10] reported full-potential linearized augmented plane wave (LAPW) calculations on fluorite platinum nitride (PtN_2). They showed the fluorite phase of platinum nitride can be mechanically stable and their calculated bulk modulus is 316 GPa using the local density approximation (LDA) exchange–correlation functional. Later studies [2, 12–14] have furthermore suggested that platinum nitride is stable in the pyrite structure with a stoichiometry of PtN_2. In the pyrite structure nitrogen atoms occupy octahedral interstitial sites of the face-centered cubic (fcc) Pt lattice. A high bulk modulus around 361 GPa, which is comparable with the experimental results, has been reported [15]. Besides, the possibility of marcasite PtN_2 has also been investigated, showing that the marcasite PtN_2 could exist as a metastable phase at pressures up to 50 GPa [16]. Furthermore, there is limited computational and experimental data on the phonon spectra of platinum nitride. Although pertinent calculations within the GGA have been reported by Young *et al* [12], giving Raman frequencies as a function of pressure, the data do not completely describe the experimental results. There is certainly a need for more theoretical and experimental studies for improvement of this aspect.

The aim of this work is to provide a comparative and complementary study to both experimental and theoretical studies on the structural, dynamical and electronic properties of platinum nitride using first-principles calculations within the density functional theory (DFT). The pseudopotential plane wave calculations of six proposed crystal structures, i.e. the zinc-blende, rock-salt, tetragonal, cuprite, fluorite and pyrite phase, have been carried out. We report structural properties such as lattice constants and bulk moduli for all these phases calculated within both the LDA and GGA. Pyrite platinum nitride (PtN_2) has the highest bulk modulus ($B = 348$ GPa), sufficiently close to the experimental value. The stability of cubic structures has also been investigated. The vibrational modes' analysis has also been performed in order to give new insights into the interpretation of Raman spectroscopic measurements. The electronic structure of pyrite PtN_2, which is shown to be mechanically stable, is discussed.

This paper is organized as follows: section 2 contains details of the computational methods used. Computed data including structural, elastic, dynamical and electronic properties of several phases are discussed in section 3 and conclusions are drawn in section 4.

2. Computational methods

The first-principles total energy and electronic structure calculations presented have been performed using the plane wave pseudopotential methods implemented in the PWSCF software package [24]. PWSCF is based on the density functional theory [25, 26] (DFT) framework with the crystalline orbitals expanded in a truncated plane wave basis, incorporating all terms with kinetic energy below a prescribed energy cutoff (E_{cut}). The kinetic energy cutoff of 408 eV and using ultrasoft pseudopotentials for platinum and nitrogen atoms [27] turns out to be sufficient for accuracy of the calculated total energy (1 meV/unit cell) of all the phases. The exchange correlation energy has been computed using the LDA parameterized by Perdew–Zunger [28] and GGA functionals by Perdew–Wang [29]. The sampling of the Brillouin zone was performed using the Monkhorst–Pack special k-point scheme [30]. We choose the k-point grids of $16 \times 16 \times 16$ for zinc-blende, rock-salt and fluorite; $12 \times 12 \times 12$ for pyrite; $10 \times 10 \times 10$ for cuprite and $12 \times 12 \times 10$ for tetragonal type structures, respectively. Tests reveal that increasing the number of k-points produces no significant difference in the computed structural parameters or energy of the crystals. All atomic coordinates were relaxed during the structural optimizations with a tolerance of 10^{-4} eV in the total energy using a modified Broyden–Fletcher–Goldfarb–Shanno (BFGS) minimization algorithm [31]. The effect of possible magnetic ground state was tested by spin polarized calculations but without including spin–orbit coupling since, as presented below, the comparison of experimental data on lattice parameters and elastic constants of heavy Pt atoms with our calculations without spin–orbit coupling results in extremely good agreement.

The total energy was computed for different volumes and the energies were fitted to the Vinet equation [32, 33]:

$$E(V,T) = E_0(T) + \frac{9B_0(T)V_0(T)}{\xi^2}\{1 + \{\xi(1-x) - 1\} \times \exp\{\xi(1-x)\}\} \quad (1)$$

where E_0 and V_0 are the zero pressure equilibrium energy and volume, respectively, $x = (V/V_0)^{1/3}$ and $\xi = \frac{3}{2}(B_0' - 1)$, $B_0(T)$ is the bulk modulus and $B_0'(T) = (\partial B(T)/\partial P)_0$. The subscript 0 alone throughout represents the standard state $P = 0$. All equations of state here are for static ($T = 0$) conditions. Pressures were obtained analytically from

$$P(V) = \frac{3B_0(1-x)}{x^2}\exp\left\{\frac{3}{2}(B_0' - 1)(1-x)\right\}. \quad (2)$$

3. Results

3.1. Structural properties

There are several crystal structures like the zinc blende, rock-salt, tetragonal, cuprite, fluorite and pyrite proposed for platinum nitride. The calculated lattice parameters, bulk modulus and its pressure derivative for all the structures considered in this paper are presented in table 1. The calculations for elemental Pt were also performed for comparison. The lattice constant and bulk modulus values obtained for bulk Pt agree very well with the experimental result [34]. We note that the LDA usually underestimates the lattice constants and overestimates the bulk modulus, while an opposite trend is seen for the GGA. For the case of fcc Pt, LDA results are found to be more accurate than the GGA ones.

Table 1. The lattice parameter (in Å), bulk modulus (in GPa) and its dimensionless pressure derivative of bulk Pt and several proposed structures of platinum nitride.

		a	c	B_0	B_0'
Exp. [1]		4.8032		372 (±5)	4.0
				354 (±5)	5.26
Zinc blende	(PtN)				
	LDA	4.692		241.515	4.97
	GGA	4.806		194.712	5.28
Rock-salt	(PtN)				
	LDA	4.410		300.158	4.89
	GGA	4.521		243.704	5.13
Tetragonal	(PtN)				
	LDA	2.914	5.623	297.908	4.40
	GGA	2.988	5.785	298.014	7.36
Cuprite	(Pt_2N)				
	LDA	4.437		231.635	5.01
	GGA	4.555		195.855	4.99
Fluorite	(PtN_2)				
	LDA	4.900		316.832	4.64
	GGA	5.002		257.341	5.30
Pyrite	(PtN_2)				
	LDA	4.778		347.818	7.20
	GGA	4.907		225.225	7.79
Bulk Pt					
	LDA	3.910		286.215	4.99
	GGA	4.007		233.427	5.22
Exp. [34]		3.924		273.6	5.23

Table 2. The compiled data from computational studies of lattice constant (in Å), bulk modulus (in GPa) and elastic constants (in GPa) of several proposed structures of platinum nitride.

		a	B_0	c_{11}	c_{12}	c_{44}
Zinc blende	(PtN)					
This work	LDA	4.692	241.5	221	252	4
Reference [6]	LSDA	4.711	231			
Reference [7]	LDA	4.722	243.3	225.2	252.3	16.8
Reference [9]	LDA	4.692	244			
Reference [11]	LDA	4.699	230	210	241	14
Reference [21]	LDA	4.743	232	315	191	50
This work	GGA	4.806	194.7			
Reference [5]	GGA	4.804	185.5			
Reference [6]	GGA	4.801	187			
Reference [7]	GGA	4.825	196.3	184.1	202.4	13.5
Reference [9]	GGA	4.780	194			
Reference [11]	GGA	4.794	192			
Reference [12]	GGA	4.760	217	197	200	22
Reference [17]	GGA	4.779	191			
Reference [18]	GGA	4.805	193	185	192	42
Rock-salt	(PtN)					
This work	LDA	4.410	300.2	383	259	41
Reference [6]	LSDA	4.429	274			
Reference [11]	LDA	4.407	284	355	248	36
Reference [21]	LDA	4.449	295	506	189	111
This work	GGA	4.521	243.7			
Reference [5]	GGA	4.518	215.7			
Reference [6]	GGA	4.521	219			
Reference [11]	GGA	4.504	226			
Reference [12]	GGA	4.471	242	266	221	36
Reference [17]	GGA	4.491	230			
Reference [18]	GGA	4.504	234	266	211	38
Fluorite	(PtN_2)					
This work	LDA	4.900	316.8	481	235	103
Reference [7]	LDA	4.943	322.1	500.3	233.0	87.2
Reference [9]	LDA	4.866	316	532	208	122
Reference [14]	LDA	4.943	321.7	499.9	232.6	87.4
Reference [20]	LDA	4.940	284.9	524.5	165.1	105.7
This work	GGA	5.002	257.3			
Reference [7]	GGA	5.040	267.2	420.2	190.7	71.5
Reference [9]	GGA	4.958	264	457	167	99
Reference [12]	GGA	4.939	260	473	160	115
Reference [14]	GGA	5.040	268.3	427.9	188.6	77.5
Pyrite	(PtN_2)					
This work	LDA	4.778	347.8	800	122	146
Reference [2]	LDA	4.790	347			
Reference [13]	LDA	4.770	352	824	117	152
Reference [15]	LDA	4.820	361	842	120	152
Reference [19]	LDA	4.806	352	824	114	154
Reference [20]	LDA	4.800	338	769	123	357
This work	GGA	4.907	225.2			
Reference [2]	GGA	4.875	278			
Reference [12]	GGA	4.848	285	696	83	136
Reference [13]	GGA	4.862	272	668	78	133
Reference [14]	GGA	4.874	297.8	689	102	129
Reference [15]	GGA	4.877	298	713	90	136

There is a large number of computational investigations of structural properties and electronic structure of platinum nitride for different proposed crystal structures [5–23]. In table 2, the lattice parameter, bulk modulus and elastic constants of cubic structures are compiled from these calculations as well as from this work. As seen in table 2, all these data reported from different calculations are in reasonable agreement. The lattice parameters calculated for the zinc-blende, fluorite and pyrite phases are very close to the experimental observations, while the ones of rock-salt and cuprite structures are generally smaller. For example, the GGA calculations predict lattice constant of zinc-blende structure in excellent agreement with the reported experimental result (within 0.04%). For the rock-salt and cuprite phases, the computed lattice parameters are underestimated approximately 8% using the LDA and 5–6% by the GGA functionals. Four more nitrogen atoms at the tetrahedral sites of the metal sublattice in fluorite PtN_2 have little effect on structural parameters. The increase, with respect to the zinc-blende structure, in the lattice constant is only within 4% by both the LDA and GGA calculations. For pyrite structure, the computed lattice parameter, a, with the LDA method agrees extremely well with the experimental result (within 0.5%).

The bulk modulus, B_0, measures the resistance to the volume change in solids and provides an estimation of the elastic response of the material to a hydrostatic pressure. Calculations of the bulk modulus of the zinc-blende phase using the LDA yield a value of 241 GPa, which is lower than the experimentally reported value of 372 GPa by 35%. The bulk modulus predicted for cuprite platinum nitride (Pt_2N) is close to that of zinc blende. For rock-salt, the computed B is reported to be somewhat higher than that of zinc-blende and cuprite phases, 300 GPa, but still off from the experimental value. The LDA calculations yield a value of 316 GPa for fluorite structure, in excellent agreement with the data reported by Yu and Zhang [9]. The significantly low bulk moduli, reported in this study for the zinc-blende, cuprite, rock-salt and fluorite phases, invalidate the probability that platinum nitride exists in such crystal structures. We obtained a B value of 348 GPa for the pyrite phase, which is about 6% lower than

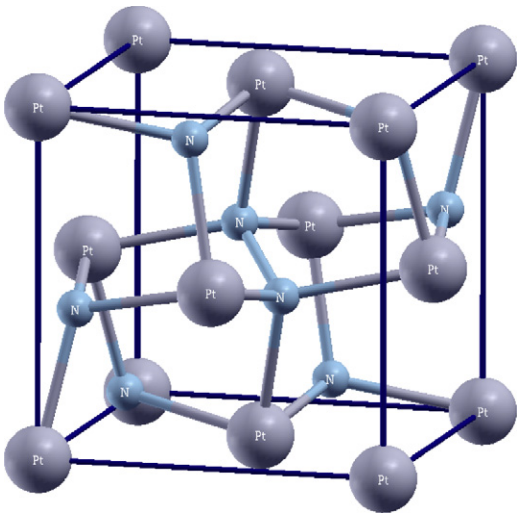

Figure 1. Unit cell of pyrite structure. Large (gray) and small (blue) spheres represent platinum and nitrogen atoms, respectively.
(This figure is in colour only in the electronic version)

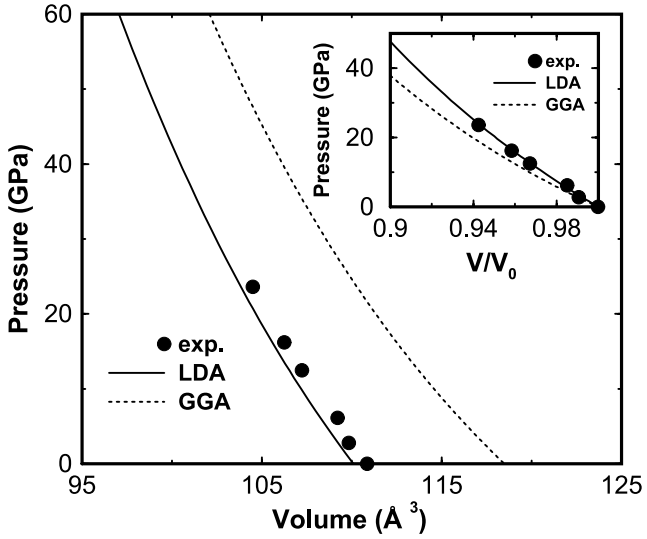

Figure 2. Equation of state (EOS) for pyrite PtN_2. LDA (solid line) and GGA (dotted line) calculations are compared with experimental data from [1]. Inset shows the EOS in terms of reduced volume, V/V_0.

that observed. By addition of experimental uncertainty there is a good consistency between the calculated value and the experimental result.

The pyrite structure, illustrated in figure 1, has a cubic unit cell in the $Pa\bar{3}$ space group. The unit cell is defined by the lattice vectors $\mathbf{a}_1 = (a, 0, 0)$, $\mathbf{a}_2 = (0, a, 0)$ and $\mathbf{a}_3 = (0, 0, a)$. Twelve atoms form the basis, four Pt atoms at $(0, 0, 0)$, $\frac{1}{2}(\mathbf{a}_1 + \mathbf{a}_2)$, $\frac{1}{2}(\mathbf{a}_1 + \mathbf{a}_3)$ and $\frac{1}{2}(\mathbf{a}_2 + \mathbf{a}_3)$ and eight N atoms at $\pm(u, u, u)$, $(\frac{1}{2} - u, -u, \frac{1}{2} + u)$, $(\frac{1}{2} + u, +u, \frac{1}{2} - u)$, $(\frac{1}{2} - u, \frac{1}{2} + u, +u)$, $(\frac{1}{2} + u, \frac{1}{2} - u, -u)$, $(-u, \frac{1}{2} + u, \frac{1}{2} - u)$ and $(+u, \frac{1}{2} - u, \frac{1}{2} + u)$. The pyrite structure is actually known as a modified or distorted fluorite structure. When $u = 1/4$ the structure reduces to the fluorite configuration. Each nitrogen atom is surrounded by six first-neighbor transition metal sites and vice versa. The lattice parameter a computed with the LDA method agree very well with the experimental result (within around 0.5%). The total energy minimum is achieved for $u = 0.43$ within both the LDA and GGA calculations.

The calculated equation of state according to the Vinet equation (equations (1) and (2)) is compared with experiment [1] in figure 2. First of all, since the lattice parameter calculated by LDA (within around 0.5%) agrees with the experimental result better than the GGA one (within around 2.0%), there is a shift in GGA EOS in the horizontal volume axis. As the inset shows, even the volume shift is corrected by presenting the EOS in terms of reduced volume (V/V_0), the LDA calculation agrees very well with the experimental result while GGA EOS deviates considerably. Hence, from lattice parameter and EOS, the LDA results are found to be more accurate than the GGA. So the results presented from now on will be based on LDA calculations unless otherwise stated.

3.2. Elastic properties and phase stability

The elastic constants determine the response of the crystal to an externally applied strain and provide information about the bonding characteristics between adjacent atomic planes, anisotropic character of the bonding and structural stability. We obtain the elastic constants at the relaxed equilibrium structure at any volume V by straining the lattice, relaxing the symmetry-allowed internal degrees of freedom and evaluating the total energy changes due to the strain as a function of its magnitude. The elastic moduli were found by fitting the energies against the distortion parameter.

The three independent moduli (c_{11}, c_{12} and c_{44}) completely describe the elastic behavior of a cubic crystal system. For cubic lattices, the bulk modulus can be expressed in terms of elastic moduli as

$$B = (c_{11} + 2c_{12})/3. \tag{3}$$

We obtain the shear constant

$$c_s = (c_{11} - c_{12})/2 \tag{4}$$

by applying the following isochoric strain [35]:

$$\epsilon(\delta) = \begin{pmatrix} \delta & 0 & 0 \\ 0 & \delta & 0 \\ 0 & 0 & (1+\delta)^{-2} - 1 \end{pmatrix}, \tag{5}$$

where δ is the magnitude of the strain. The corresponding strain energy is

$$E(\delta) = E(0) + 6c_s V\delta^2 + \mathrm{O}(\delta^3). \tag{6}$$

By calculating the bulk modulus and the shear constant, it is possible to extract c_{11} and c_{12}. To determine c_{44} we use the orthorombic strain:

$$\epsilon(\delta) = \begin{pmatrix} 0 & \delta & 0 \\ \delta & 0 & 0 \\ 0 & 0 & \delta^2/(1-\delta^2) \end{pmatrix} \tag{7}$$

Table 3. Single-crystal elastic constants c_{ij} and isotropic (aggregate) elastic moduli of bulk Pt and several phases of platinum nitride. All elastic constants are in GPa, except the dimensionless anisotropy ratio A and Poisson's ratio ν. All results are based on LDA calculations.

	c_{11}	c_{12}	c_{44}	A	B	G	Y	ν
Bulk Pt	355	252	81	1.57	286	68	188	0.391
Zinc blende (PtN)	221	252	4	−0.26	242	2	6	0.496
Rock-salt (PtN)	383	259	41	0.66	300	48	138	0.423
Cuprite (Pt_2N)	232	234	−44	44	232	−15	−45	0.532
Fluorite (PtN_2)	481	235	103	0.84	317	111	297	0.344
Pyrite (PtN_2)	800	122	146	0.43	348	206	516	0.253

leading to the corresponding total energy:

$$E(\delta) = E(0) + 2c_{44}V\delta^2 + \mathrm{O}(\delta^4). \tag{8}$$

To date, no direct experimental moduli are available to be compared with our theoretical results. In order to probe our calculation method, bulk Pt have also been investigated. Because the data for bulk Pt compare remarkably well with experiments (347, 251 and 76.5 GPa for c_{11}, c_{12} and c_{44}, respectively [36]), our results can be considered as a reliable prediction for the elastic properties of all treated platinum nitride structures.

The complete set of elastic moduli for cubic zinc-blende, rock-salt, cuprite, fluorite, and pyrite structures at ambient condition are listed in table 3. Our elastic constants calculations for pyrite PtN_2 are in good agreement with the results of Yu *et al* [13] as shown in table 2. The anisotropy ratio $A = c_{44}/c_s$ is also presented in table 3. While bulk Pt exhibits a typical value of 1.57, the anisotropy ratio of pyrite PtN_2 is as small as 0.43.

The requirement of mechanical stability in a cubic crystal leads to the following restrictions on the three elastic constants:

$$\begin{gathered}(c_{11} - c_{12}) > 0, \qquad c_{11} > 0, \qquad c_{44} > 0, \\ (c_{11} + 2c_{12} > 0).\end{gathered} \tag{9}$$

Our results reveal that zinc-blende and cuprite phases are not stable structures. The whole set of c_{ij} obtained for rock-salt, fluorite and pyrite phases satisfies all the above conditions, indicating a certain mechanical stability.

Hardness is commonly defined as the resistance of a material to deformations. Using the correlation between the bulk modulus and the hardness, many theoretical predictions on hard materials have been made during the last few decades. However, Lèger *et al* [37] confirm the shear modulus (G) as the best hardness predictor for a wide variety of materials. The magnitude of G describes the resistance of a material upon shape change and plays an important role in the elasticity theory. For polycrystalline sample, the average isotropic shear modulus G and bulk modulus B can be determined from single-crystal elastic constants according to the Voigt–Reuss–Hill scheme [38]. The calculated shear moduli validate the same hardness trend as found with the estimated bulk modulus. The relatively large bulk modulus and high hardness in the pyrite PtN_2 phase are favorable for potential hard-device applications.

Table 4. The upper part shows the solution of wave equation ($\rho v^2 = \bar{c}$) in three directions in a cubic lattice. ((⋆) polarized along [001] and (⋆⋆) polarized along [$1\bar{1}0$].) The middle part is the longitudinal and transverse sound velocities in units of (m s^{-1}) for bulk Pt and pyrite platinum nitride, while the lower part includes the aggregate sound velocities.

Mode	[100]	[110]		[111]
Longitudinal	c_{11}	$(c_{11} + c_{12} + 2c_{44})/2$		$(c_{11} + 2c_{12} + 4c_{44})/3$
Transverse	c_{44}	c_{44}	(⋆)	$(c_{11} - c_{12} + c_{44})/3$
		$(c_{11} - c_{12})/2$	(⋆⋆)	
Bulk Pt				
Longitudinal	4047	4212		4265
Transverse	1933	1933;	1541	1682
Pyrite (PtN_2)				
Longitudinal	7674	6684		6320
Transverse	3278	3278;	4995	4496
Aggregate	v_P	v_S		v_B
Bulk Pt	4167	1765		3634
Pyrite (PtN_2)	6771	3895		5061

The Young's modulus Y, and Poisson's ratio ν are two important quantities for technological and engineering applications and provide a fundamental description of a material's mechanical behavior. For cubic lattices, Poisson's ratio ν can be expressed as $\nu = (3B - 2G)/(6B + 2G)$ and the Young's modulus Y is calculated from $Y = 2G(1 + \nu)$. The calculated aggregate elastic moduli of all the considered structures of platinum nitride are listed in table 3.

Sound velocities are related to the elastic constants by the Christoffel equation [39]

$$(c_{ijkl}n_j n_k - \rho v^2 \delta_{ij})u_i = 0, \tag{10}$$

where c_{ijkl} is the elastic constants tensor, ρ is the density, $\vec{n}$ is the propagation direction, $\vec{u}$ is the polarization vector and v is the velocity. Solutions [40] of this wave equation for a cubic lattice are summarized in three major directions in table 4. Moreover, isotropically averaged aggregate velocities are given by $v_P = ((B + 4/3G)/\rho)^{1/2}$, $v_S = (G/\rho)^{1/2}$ and $v_B = (B/\rho)^{1/2}$, where v_P, v_S and v_B are the compressional, shear and bulk sound velocities. The aggregate velocity of compressional, shear and bulk waves are presented for bulk Pt and pyrite PtN_2 in table 4.

3.3. Dynamical properties

Since the Raman spectroscopy is one of the major identification tools at the reported experiments [1, 2] and in general for pressure-induced changes of different structural phases, we calculated phonon band structures for various platinum nitride structures and, especially, the Raman-active phonon modes are analyzed and compared in detail. Moreover, the knowledge of phonon frequencies and eigenvectors is an indispensable step for further investigation of interesting properties such as specific heat, phonon-assisted photoemission, thermal expansion and thermal conductivity. We employed the formalism of density functional perturbation theory [41] (DFPT) within the local density approximation for

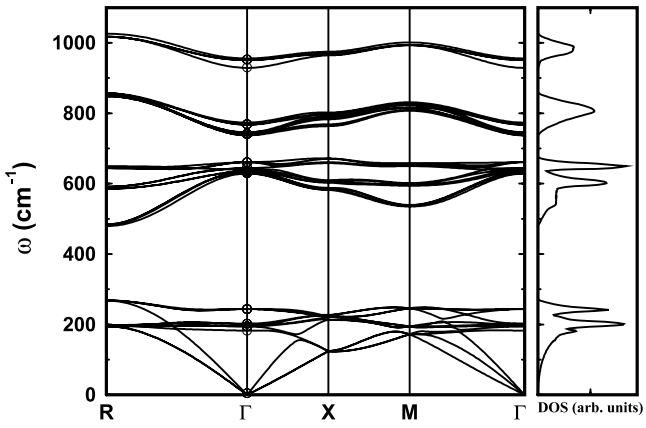

Figure 3. Calculated phonon dispersion curves along high symmetry directions in the Brillioun zone as well as the phonon density of states (DOS) for pyrite PtN_2. The frequencies from DFPT calculation at Γ-points are included as open circles in order to compare results of different methods.

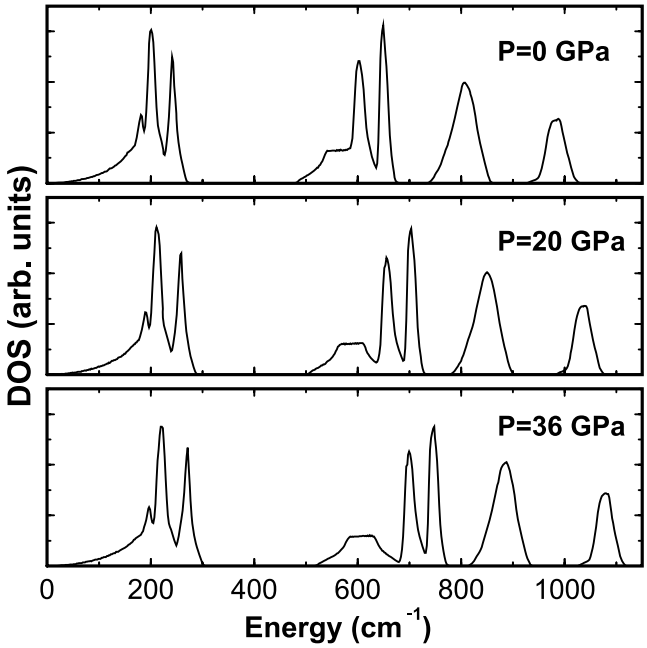

Figure 4. Calculated phonon density of states (DOS) at three different hydrostatic pressures (0, 20 and 36 GPa) for pyrite PtN_2.

the calculation of the phonon spectrum of zinc-blende, rock-salt, fluorite and pyrite structures. The calculations show that zinc-blende and rock-salt structures are dynamically unstable because the computed phonon dispersion relations include several imaginary frequencies. However, there are no soft modes appearing either for fluorite or pyrite structures, hence these structures are dynamically stable. The calculated Raman-active phonon frequency of fluorite structure at zone center is 536 cm^{-1}, which is slightly lower than that reported by Yu and Zhang [10] (≈628 cm^{-1}). This discrepancy might originate from anharmonic effects, neglected in our calculations.

Eventually, the vibrational properties of pyrite PtN_2 are investigated in detail. In addition to the DFPT calculations, we have also performed the direct force constant method with small displacement [42] (SDM) for the construction of dynamical matrix and phonon calculations of pyrite PtN_2. For SDM calculations, a 2 × 2 × 2 supercell is formed and the resulting forces on the atoms are checked after displacing the atoms within the unit cell from their equilibrium positions by various amounts. This way, effects like linearity and anharmonicity are all tested. Consequently, a rather small displacement such as $\delta \approx 0.005$ Å is used for force and dynamical matrix calculations. Figure 3 shows the calculated phonon dispersion curves along high symmetry directions as well as the phonon density of states for the pyrite phase. In order to benchmark the different methods and approximations, the frequencies from DFPT calculation at Γ-points are presented as open circles in figure 3. This clearly exhibits that SDM frequencies are almost identical to the DFPT ones.

Considering the fact that the platinum nitride was synthesized using the laser-heated diamond anvil cell set-up and then it was first characterized by Raman spectroscopy at pressures around 50 GPa, we have investigated the vibrational properties of pyrite PtN_2 under three different uniform pressures, namely 0, 20 and 36 GPa. The phonon density of states (DOS) at three different hydrostatic pressures are presented in figure 4. The phonon band structure shown in figure 3 and the phonon DOS illustrated in figure 4 clearly demonstrate four well-separated phonon bands with bandgaps. The peaks around 200 cm^{-1} at phonon DOS are due to the relatively soft optical modes which are IR-active that overlap with acoustical modes. As seen from figure 4, all frequencies are only shifted to higher energies without significant changes in lineshape with increasing pressure.

Table 5. The frequencies of Raman-active modes at the zone center (Γ-point) in units of cm^{-1} for pyrite structure.

		Phonon frequencies (cm^{-1})				
Exp [1]			743		862	892
Exp [2]		676	743		860	891
This work DFPT	LDA	740	742	768	930	952
This work SDM	LDA	737	745	767	928	951
Reference [2]	GGA	735	741	759	900	928
Reference [12]	GGA	689	695	710	854	885
Reference [43]	LDA	720	727	751	929	958

Next, we summarize the Raman-active zone-center modes of pyrite PtN_2 and compare them with the available experimental data and other computational results in table 5. There are five Raman-active modes in pyrite crystal structure [43]. However, only four modes were clearly identified and reported from Raman spectroscopy measurements [1, 2]. When we compare this experimental data with the calculated frequencies, there is only a partial match with some of the modes for the given calculated dataset. For example, two high energy modes agree perfectly with the results of Young *et al* [12], while the mode at 743 cm^{-1} coincides with this work's result as well as that of [2]. For this reason, we compare the available calculated frequencies in detail as well. First of all, there is perfect agreement between our calculated frequencies from two different methods, i.e. DFPT and SDM results. These frequencies agree

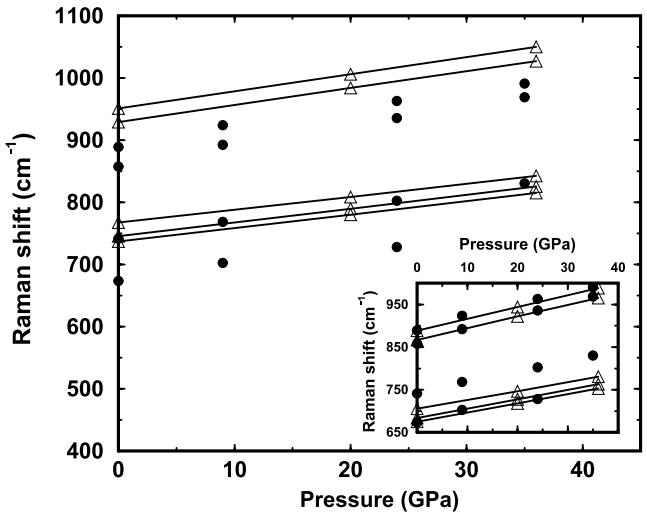

Figure 5. Calculated Raman shifts as a function of uniform pressure for pyrite PtN_2. Solids circles are the experimental data from [1]. Inset shows the same graph where the calculated frequencies are shifted downwards by 60 cm^{-1} in order to exhibit the match with the experimental data.

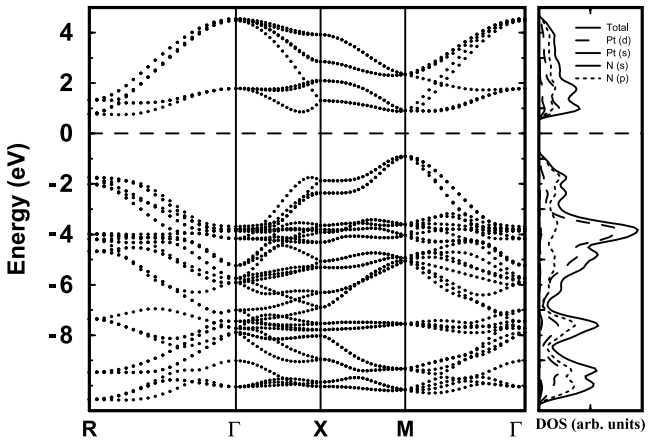

Figure 6. Energy band structure of pyrite PtN_2 along high symmetry directions within the Brillouin zone. Some of the important LDOS contributions to TDOS are shown in the right panel.

very well with the ones which are calculated within the LDA by Meier and Weihrich [43], even though the shift between the corresponding frequencies is as high as 20 cm^{-1} for lower frequency modes. On the other hand, the frequencies computed within the GGA by Young *et al* [12] are significantly lower than ours, but the ones from [2], especially around 750 cm^{-1}, agree well. The reason of this discrepancy between these two calculations within the GGA is that, while the former one was performed at a theoretical equilibrium lattice constant (4.848 Å), the latter one was computed at an experimental lattice constant (4.80 Å).

In order to make a better comparison of experimental Raman frequencies with the calculated ones, the Raman shifts as a function of pressure are presented in figure 5. In this pressure range between 0 and 36 GPa, the frequencies of Raman-active modes increase linearly with increasing pressure like the experimental reported ones [1], shown by solid circles in figure 5. However, there is an appreciable difference between the absolute values of calculated and experimental frequencies. In order to quantify this, we shifted the calculated frequencies downwards by 60 cm^{-1} and replotted the same graph as illustrated in the inset. This way, now there is an excellent agreement between the calculated and experimental two topmost and lowest energy Raman modes. Still, there is no match for the mode around 743 cm^{-1} and one mode (probably around the lowest energy Raman mode) was not resolved in the experiments.

These lattice dynamical calculations have provided some additional insight for vibrational properties of platinum nitride. This work provides reliable and detailed *ab initio* phonon frequencies of platinum nitride. However, all of the calculated pyrite phonon modes do not sufficiently cover the experimental Raman spectra. Therefore, there is still a need for further studies on this aspect.

3.4. Electronic structure

In order to investigate the electronic properties of platinum nitride we have analyzed the density of states (DOS) and band structure of pyrite PtN_2. Figure 6 illustrates the electronic band structure along some high symmetry directions within the cubic Brillouin zone and the total DOS in the unit cell. The present calculations in the framework of the LDA has yielded a small indirect gap of 1.66 eV, in agreement with the experiment as well as other calculations. The indirect gap of PtN_2 is found to increase with increasing pressure as in the case of diamond. The valence band maximum is located at the M point, and the lowest conduction state lies along the Λ direction. Furthermore, one can conclude from DOS that the valence band edge shows mainly N p-orbital character while the major peak of DOS within the valence band around 4 eV below the Fermi level is due to the Pt d-orbitals. Along the rest of the valence band as well as the conduction band edge one can see mainly the contribution of Pt d-orbital and N p-orbitals. To gain more insight about the atomic bonding in pyrite PtN_2, we have examined the charge density, which indicates a strong covalency in the interstitial dinitrogen units. The strong directional bonding between Pt–N might contribute to the hardness of platinum nitride.

4. Conclusions

In this work, we have studied the six proposed crystal structures (zinc blende, rock-salt, tetragonal, cuprite, fluorite and pyrite) of platinum nitride by the first-principles plane wave pseudopotential calculations both with LDA and GGA functionals in order to investigate the mechanical, dynamical and electronic properties. We have obtained highly converged total energies, forces and stresses in all structures.

Our calculated lattice constant and bulk modulus for pyrite PtN_2 obtained using the LDA agree well with the experimental values. Our results indicate that pyrite PtN_2 has the highest bulk modulus at 348 GPa. The equation of state (EOS) for pyrite structure reveals the excellent agreement between LDA

calculations and experimental results, which points out the essentiality of using the LDA. We computed elastic constants of cubic structures using volume-conserved tetragonal and orthorombic stresses. The results demonstrate that only zinc blende and cuprite are mechanically unstable. The analysis of the complete set of elastic moduli for the pyrite phase shows how the PtN_2 stoichiometry leads to the formation of hard platinum nitride. The pyrite phase has a very large shear modulus of $G = 206$ GPa, which is about three times the value for the elemental Pt. Considering the correlation between the hardness and the shear modulus, the enhancement in hardness is quite remarkable. In addition, the calculated electronic band structure of pyrite PtN_2 yield an indirect bandgap of 1.66 eV.

We have analyzed the phonon dispersion relations of the platinum nitride. These lattice dynamical calculations have provided some additional insight in stability and vibrational properties of platinum nitride. The calculations show that zinc-blende and rock-salt structures are dynamically unstable. On the other hand, there are no soft modes appeared either for fluorite or pyrite structures, hence these structures are dynamically stable as well. Since pyrite PtN_2 seems to be a potential candidate to explain the formation of hard platinum nitride, its phonon modes, especially the Raman modes, are discussed in detail. The calculated vibrational modes of pyrite PtN_2 do not show complete agreement with experimental Raman frequencies.

Our results for pyrite PtN_2 compare remarkably well with experiments; these can be considered as a reliable prediction for structural, dynamical and electronic properties of platinum nitride. However, we believe that more experimental and theoretical studies are required to make a conclusive decision about the nature of the platinum nitride material. The current study serves to underpin further investigation of synthesis and characterization of possible noble metal nitrides and provides a useful information for potential hard material applications.

Acknowledgments

This work was partially supported by the TR-ACCESS Project subprogram of The Scientific and Technological Research Council of Turkey, TÜBİTAK, and OG acknowledges the support of the Turkish Academy of Sciences, TÜBA.

References

[1] Gregoryanz E, Sanloup C, Somayazulu M, Bardo J, Fiquet G, Mao H-K and Hemley R J 2004 *Nat. Mater.* **3** 294
[2] Crowhurst J C, Goncharov A F, Sadigh B, Evans C L, Morall P G, Ferreira J L and Nelson A J 2006 *Science* **311** 1275
[3] Young A F, Sanloup C, Gregoryanz E, Scandolo S, Hemley R J and Mao H-K 2006 *Phys. Rev. Lett.* **96** 155501
[4] Yakovenk E V, Aleksandrov I V, Goncharov A F and Stishov S M 1989 *Sov. Phys.—JETP* **68** 1213
[5] Sahu B R and Kleinman L 2005 *Phys. Rev.* B **71** 041101(R)
Sahu B R and Kleinman L 2005 *Phys. Rev.* B **71** 209904(E)
Sahu B R and Kleinman L 2005 *Phys. Rev.* B **72** 119901(E)
[6] Uddin J and Scuseria G E 2005 *Phys. Rev.* B **72** 035101
Uddin J and Scuseria G E 2005 *Phys. Rev.* B **72** 119902(E)
[7] Fan C Z, Sun L, Wang Y, Wei Z, Liu R, Zeng S and Wang W 2005 *Chin. Phys. Lett.* **22** 2637
[8] Kanoun M B and Goumri-Said S 2005 *Phys. Rev.* B **72** 113103
[9] Yu R and Zhang X F 2005 *Appl. Phys. Lett.* **86** 121913
[10] Yu R and Zhang X F 2005 *Phys. Rev.* B **72** 054103
[11] Patil S K R, Khare S V, Tuttle B R, Bording J K and Kodambaka S 2006 *Phys. Rev.* B **73** 104118
[12] Young A F, Montoya J A, Sanloup C, Lazzeri M, Gregoryanz E and Scandolo S 2006 *Phys. Rev.* B **73** 153102
[13] Yu R and Zhang X F 2006 *Appl. Phys. Lett.* **88** 051913
[14] Fan C, Zeng S, Li L, Zhan Z, Liu R, Wang W, Zhang P and Yao Y 2006 *Phys. Rev.* B **74** 125118
[15] Gou H, Hou L, Zhang J, Sun G, Gao L and Gao F 2006 *Appl. Phys. Lett.* **89** 141910
[16] Chen Z W, Guo X J, Liu Y, Ma M Z, Jing Q, Li G, Zhang X Y, Li L X, Wang Q, Tian Y J and Liu R P 2007 *Phys. Rev.* B **75** 054103
[17] Yu L H, Yao K L, Liu Z L and Zhang Y S 2007 *Physica* B **399** 50
[18] Peng F, Fu H and Yang X 2008 *Physica* B **403** 2851
[19] Fu H, Liu W F, Peng F and Gao T 2009 *Physica* B **404** 41
[20] Bettahar N, Benalia S, Rached D, Ameri M, Khenata R, Baltache H and Rached H 2009 *J. Alloys Compounds* **478** 297
[21] Rabah M, Rached D, Khenata R, Moulay N and Zenati A 2009 *Solid State Commun.* **149** 941
[22] Aberg D, Sadigh B, Crowhurst J and Goncharov A F 2008 *Phys. Rev. Lett.* **100** 095501
[23] Zhang X, Trimarchi G and Zunger A 2009 *Phys. Rev.* B **79** 092102
[24] PWSCF software package: http://www.pwscf.org
[25] Hohenberg P and Kohn W 1964 *Phys. Rev.* **136** B864
[26] Kohn W and Sham L J 1965 *Phys. Rev.* **140** A1133
[27] Vanderbilt D 1990 *Phys. Rev.* B **41** 7892
[28] Perdew J P and Zunger A 1981 *Phys. Rev.* B **23** 5048
[29] Perdew J P and Wang Y 1992 *Phys. Rev.* B **45** 13244
Perdew J P and Wang Y 1992 *Phys. Rev.* B **46** 6671
[30] Monkhorst H J and Pack J D 1976 *Phys. Rev.* B **13** 5188
[31] Fischer T H and Almlof J 1992 *J. Phys. Chem.* **96** 9768
Schlegel H B 1982 *J. Comput. Chem.* **3** 214
[32] Vinet P, Ferrante J, Smith J R and Rose J H 1986 *J. Phys. C: Solid State Phys.* **19** L467
Vinet P, Rose J H, Ferrante J and Smith J R 1989 *J. Phys.: Condens. Matter* **1** 1941
[33] Cohen R E, Gülseren O and Hemley R J 2000 *Am. Mineral.* **85** 338
[34] Dewaele A, Loubeyre P and Mezouar M 2004 *Phys. Rev.* B **70** 094112
[35] Gülseren O and Cohen R E 2002 *Phys. Rev.* B **65** 064103
[36] Simmons G and Wang H 1971 *Single Crystal Elastic Constants and Calculated Aggregate Properties: A Handbook* (Cambridge, MA: MIT Press)
[37] Lèger J M, Djemia P and Ganot F 2001 *Appl. Phys. Lett.* **79** 2169
[38] Hill R W 1952 *Proc. Phys. Soc. Lond.* A **65** 349
[39] Christoffel E B 1877 *Ann. Math. Pura Appl.* **8** 193
[40] Grimvall G 1986 *Thermophysical Properties of Materials* (Amsterdam: North-Holland)
[41] Baroni S, de Gironcoli S, Dal Corso A and Giannozzi P 2001 *Rev. Mod. Phys.* **73** 515
[42] Kresse G, Furthmüller J and Hafner J 1995 *Europhys. Lett.* **32** 729
[43] Meier M and Weihrich R 2008 *Chem. Phys. Lett.* **461** 28